analytical chemistry

pubs.acs.org/ac Article

Laser Ablation Electrospray Ionization Achieves 5 μm Resolution Using a Microlensed Fiber

Yifan Meng,[†] Xiaowei Song,[†] and Richard N. Zare*

Cite This: https://doi.org/10.1021/acs.analchem.2c01942 Read Online

ACCESS | Metrics & More | Article Recommendations | Supporting Information

ABSTRACT: A pulsed (10 Hz) infrared (IR) (1064 nm) laser is focused on a sample surface by means of a microlensed fiber. Analytes desorbed from the surface are captured by charged microdroplets before entering a mass spectrometer. By translating the sample surface, a chemical map is generated with a resolution of 5 μm, defined as the change from 20 to 80% of the analyte signal intensity. As a demonstration of the power of this new imaging technique, analytes from a parsnip root section are imaged and compared with that obtained from conventional laser ablation electrospray ionization mass spectrometry. The improvement in spatial resolution is about a factor of 20.

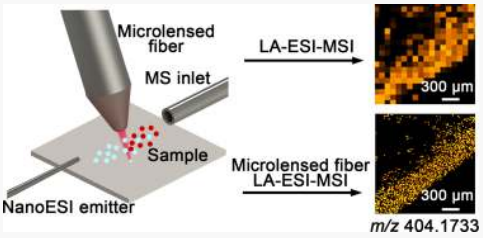

Mass spectrometry imaging (MSI) allows visualizing the distribution of different chemicals in a variety of samples, especially biological tissues.[1−4] Unlike conventional optical imaging techniques, MSI does not require tissue staining or labeling of target molecules.[5−7] Instead, desorption and ionization of molecules from a sample surface are key steps. Electrospray ionization (ESI) is an efficient soft ionization approach for detecting multiple molecules.[8,9] Desorption electrospray ionization (DESI) developed from ESI is also a commonly used MSI technique, in which the surface being analyzed is impacted by charged droplets of solvent generated from an electrospray.[10−12] However, the spatial resolution remains a challenge for DESI because of the large sampling spot size by electrospray.[13] The spatial resolution in DESI-MSI is typically about 150 μm. To tackle this spatial limitation, the Akos Vertes group has introduced another ambient electrospray-based MSI technique, called laser ablation electrospray ionization mass spectrometry (LA-ESI-MS).[14−17] In this process, analytes on the sample surface are first desorbed mostly in the neutral form by a focused laser beam (usually mid-infrared (mid-IR)). After colliding with charged droplets from the electrospray source, analytes will be ionized and transmitted into the heated inlet of a mass spectrometer and the resulting ions are sorted by their mass-to-charge ratios. The typical spatial resolution of LA-ESI-MSI is about 100 μm. It might be imagined that the resolution might be as small as the diffraction limit of the laser spot, but lens aberration and the long working distance of the experimental setup make this less possible. While the spatial resolution can be increased by employing near-field optical techniques,[18] or using a vacuum ultraviolet (VUV)[19] or extreme ultraviolet (EUV)[20] laser and transmission geometry optical systems,[2,21,22] the complexity of these approaches makes it difficult to combine ESI with these laser-sampling methods to achieve high-spatial-resolution MSI under ambient conditions.

In the following, we describe an improved high-spatial-resolution LA-ESI-MSI technique using a microlensed fiber, which has been developed previously.[5,23,24] The distance between the fiber microlens and the sample surface was able to be reduced to only several microns. In this way, sampling craters near the optical diffraction limit were able to be achieved. It is worth mentioning that the Akos Vertes group has already introduced the use of optical fiber in LA-ESI-MS.[25] A chemically etched fiber (450 μm core diameter) was used to transfer the laser onto the sample surface. Using this method, an ∼30 μm ablation spot can be obtained on onion epidermal cells.[26] In this study, the microlensed fiber (16 μm core diameter) was fabricated by mechanical polishing and could achieve a more accurate laser focusing effect. To obtain the highest signal intensity, the *X*-distance (from sampling spot to electrospray emitter in the horizontal direction) and *Z*-distance (from the sample surface to mass spectrometer inlet in the vertical direction) were accurately optimized. With the mass spectra intensity line scan of a standard grid sample, the spatial resolution was calculated to be ∼5 μm, which seems to be the highest level among the reported LA-ESI-MSI methods. We performed both traditional LA-ESI-MSI and microlensed fiber desorption ESI-MSI on the same parsnip root tissue slice to demonstrate the imaging improvement with this high-resolution technique.

Received: May 3, 2022
Accepted: June 28, 2022

EXPERIMENTAL SECTION

Microlensed Fiber Desorption ESI-MSI Platform. Compared with traditional LA-ESI-MS, we replaced the laser focusing device with a microlensed fiber, which was used to transmit and precisely focus the pulsed laser output onto the sample surface. Figure 1 presents a schematic diagram of the microlensed fiber desorption ESI-MSI platform. The sample was fixed on a two-dimensional micropositioner (Micro-Stage systems, Mad City Labs, Inc., Madison, WI). An ion transfer tube with a 50 mm extension is mounted on the mass spectrometer (Orbitrap Elite Velos Pro, Thermo Fisher) as the MS inlet. To ensure high ion transfer efficiency, a cylinder-shaped ceramic heater (Xinxinshiji, Inc., Beijing, China) with a 2 mm inner diameter and a 40 mm length was placed on the periphery of the ion transfer tube and the temperature was set as 250 °C. A self-assembled nanoESI emitter (MicroTee Peek 360 μm, IDEX Health & Science, LLC, WA) that has a fused quartz capillary tip (I.D. 75 μm and O.D. 375 μm, Polymicro) with an aperture diameter of ~1 μm was used to generate the charged droplets. The flow rate of the solvent (methanol and water, v/v = 1:1) and ESI voltage were set to 100 nL/min and 1.6 kV, respectively, to ensure steady and continuous electrospray generation. The pure silica fiber with a mode field diameter of 16 μm (FM SI-2-ULL, Yangtze Optical Fiber Company, Wuhan, China) was ground to produce a microlens with a 10 μm radius of curvature. A linear micropositioner (Micro-Stage systems, Mad City Labs, Inc., Madison, WI) was used to control the distance between the sample surface and the microlensed fiber to obtain the best focusing condition. The angle between the microlensed fiber and the sample surface is 45°. A nanosecond neodymium-doped yttrium aluminum garnet (Nd-YAG) laser (wavelength 1064 nm, DCR-11, Spectra-Physics) was coupled into the fiber with a lens (f = 20 mm) and focused on the sample surface for analyte desorption. A charge-coupled device (CCD) camera was used for the real-time observation of the imaging area. The photograph of the ion source is shown in Figure S1, and the exact drawing of the ion source is shown in Figure S2.

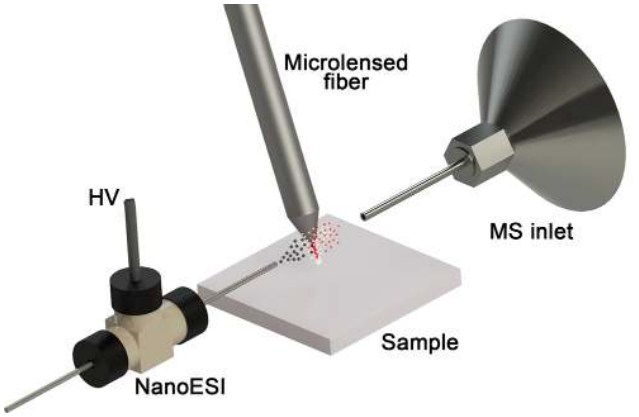

Figure 1. Schematic diagram of the LA-ESI-MSI platform with a microlensed fiber.

RESULTS AND DISCUSSION

Optimization of Ion Source Parameters. Because high-spatial-resolution imaging requires a high MS detection sensitivity, it is desirable that as many ions as possible will be produced through the sampling process. Therefore, two important parameters, the X-distance (from sampling spot to electrospray emitter in the horizontal direction) and Z-distance (from the sample surface to mass spectrometer inlet in the vertical direction), were accurately optimized. Figure 2a shows the schematic diagram of optimization, which used rhodamine B as the sample analyte. The distance between mass spectrometry inlet and nanoESI emitter was set as 8 mm. The single pulse energy of the laser and the distance between microlensed fiber and sample surface were set as 1.5 μJ and 8 μm, respectively. As shown in Figure 2b, the signal intensity of rhodamine B of a single laser pulse shows large differences with different X and Z distances. In this technique, the desorption and ionization processes of the sample are separated by laser and electrospray. To obtain the highest signal intensity, we desire to obtain the largest collision cross section of laser ablation plume and electrospray plume. Through the signal intensity evolution, the best conditions for X and Z distances were 0.5 and 2.0 mm, which was used in the following MSI experiments.

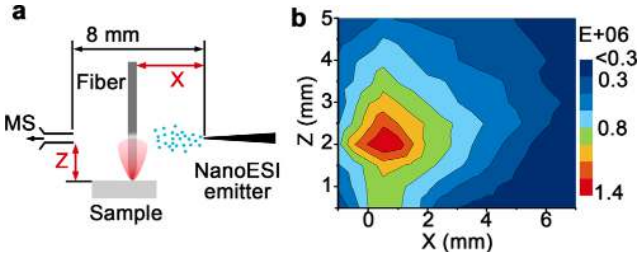

Figure 2. Optimization of ion source parameters. (a) Schematic diagram showing the X and Z distances. (b) Signal intensity of rhodamine B at different X and Z distances.

In a typical microlensed fiber desorption electrospray ionization process, the laser was considered as the sample desorption source rather than the ionization source. That is, we used a laser with low pulse energy to make sure that the laser only desorbs the molecules from the solid sample surface to the gas phase. Then, the neutral molecules are efficiently ionized by the collision with charged droplets produced by the nanoESI emitter. In this way, the signal interference caused by the laser desorption ionization (LDI) process can be greatly avoided. Also, the lower laser energy density guaranteed a smaller sampling spot. We placed on a glass slide a 5 μL drop of rhodamine B and of reserpine, each at a concentration of 1 mM in methanol. After the solvent evaporated, the glass slide was mounted on the two-dimensional micropositioner. As shown in Figure 3, when there was only the laser or ESI applied, the ion signal of the analyte cannot be detected (orange and green lines in the mass spectra). When both laser and ESI were turned on, the ion signal of rhodamine B at m/z = 443.2334 and reserpine at m/z = 609.2819 can be observed. This study demonstrated that ions were generated by laser ablation combined with electrospray capture.

A previous study has indicated that an adjustable sampling area is able to be achieved by changing the laser energy and the distance between the microlensed fiber and sample surface.[23] In this process, the distance between the fiber and sample surface is able to be clearly observed by the CCD camera (Figure S2). We prepared a rhodamine B cladding sample on a glass slide by vacuum sublimation. By adjusting the laser desorption conditions, we studied the intensity and stability of

https://doi.org/10.1021/acs.analchem.2c01942
Anal. Chem. XXXX, XXX, XXX−XXX

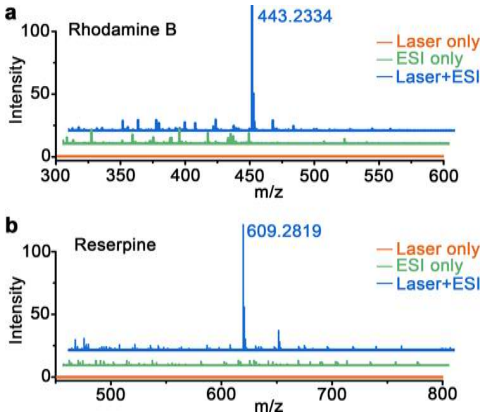

Figure 3. Mass spectra of (a) rhodamine B and (b) reserpine under different ion source configurations. The orange line shows the spectra with only the laser on. The green line shows the spectra with only the ESI on. The blue line shows the spectra of a combination of laser and ESI both on.

the rhodamine B signal with different sampling crater sizes. As shown in Figure 4a, sampling craters of different sizes can be

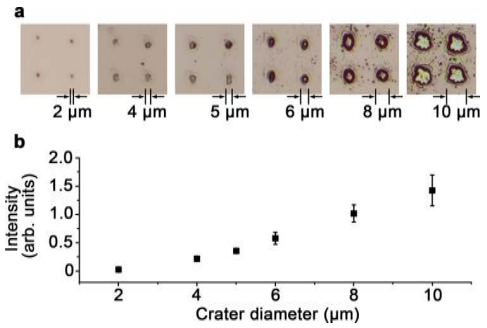

Figure 4. (a) Sampling craters of different sizes on a rhodamine B film on a silica substrate. (b) Rhodamine B mass spectrum signal intensity for different sizes of sampling craters obtained with a single laser pulse. Each error bar represents one standard deviation (n = 4).

obtained by changing the laser pulse energy and the distance between fiber and sample surface. The single pulse energies required to get the ablated craters from left to right are about 200, 340, 550, and 780 nJ, and 1 and 1.5 μJ, while the required distances between the fiber tip and the sample surface are about 15, 13, 13, 10, 10, and 8 μm. The size of the sampling crater is the most intuitive representation of the spatial resolution of the MSI. Smaller sampling craters allow for a more precise laser scan and a higher resolution. However, due to the ionization efficiency and ion loss during the transfer process, the reduced signal intensity limits the spatial resolution. Figure 4b shows the mass spectra signal intensity of rhodamine B at m/z = 443.2334 of a single laser pulse with different sampling sizes. When the crater diameter is about 10 μm, a strong signal can be obtained. As the crater diameter and sampling amount decrease, the signal intensity also becomes lower. Sampling craters with a diameter of 5 μm are considered to be the limiting resolution based on spatial resolution and signal intensity.

Evaluation of the Spatial Resolution. Generally, the spatial resolution of MSI is considered to be the distance between 20 and 80% amplitude change of the line-scan profile on a sharp edge.[20] We made a shape-standard grid sample by sublimating rhodamine B on a gold transmission electron microscopy (TEM) grid (01824G, 300 mesh, Ted Pella, Inc., Redding, CA). Figure 5a shows the sample preparation

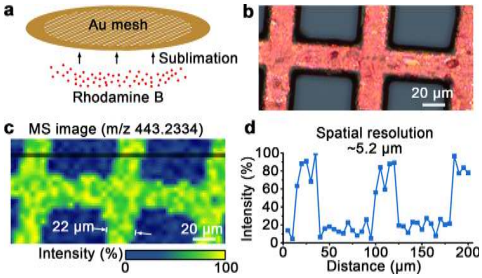

Figure 5. Evaluation of spatial resolution of microlensed fiber LA-ESI-MSI. (a) Schematic diagram of rhodamine B grid sample preparation. (b) Optical image of the imaging area on the rhodamine B grid sample. (c) MS image of rhodamine B $[C_{28}H_{31}N_2O_3]^+$ at m/z = 443.2334 of the area in (b). (d) Signal intensity scan of the black line in (c).

process. In a 100 μm × 200 μm area (Figure 5b), we performed the high-resolution MSI. The sample moving step size was set as 5 μm, and each pixel represents the rhodamine B signal at m/z = 443.2334 obtained with a single laser pulse. Figure 5c shows the imaging result consistent with the optical image. By choosing a sharp edge in the outlined part in Figure 5c, the imaging resolution is revealed to be approximately 5 μm (Figure 5d). Additionally, we used a marker pen to draw a pattern on a glass slide and perform LA-ESI-MSI within an area of 240 μm × 210 μm. The results showed that the main ingredient of the marker pen is also rhodamine B. After laser scanning, the sampling craters could be clearly observed on the surface (Figure S3).

High-Resolution Plant Root Imaging. Over the past decade, MSI has been adopted for the investigation of plant biology, including mechanisms of plant responses to stresses both abiotic and biotic, plant defense mechanisms, beneficial symbiotic relationships, and fundamental eco-physiologically important processes including nitrogen fixation and nutrient cycling.[27] For example, researchers have proved that LA-ESI-MS is able to detect chemical distributions in plant tissues, such as leaves and roots.[17,28−30] However, because of the limitation of spatial resolution, traditional LA-ESI-MSI can only visualize metabolites of plants on a macroscopic scale. We use microlensed fiber LA-ESI-MSI to explore the location of multiple metabolites in a parsnip root. To demonstrate the advantage of high-resolution imaging, we recorded MSI images with different spatial resolutions and compared them, side by side, with the traditional approach. The high-resolution imaging makes little damage to the sample, so it does not affect the low-resolution imaging experiment in the same area, which is taken again. The parsnip root was cut into 100 μm-thick slices by a freezing microtome (HM525 NX, Thermo Scientific, Waltham, MA) without any treatment (Figure 6a). To minimize signal interference, cryo-gel embedding medium was only used for fixing a plant sample from its bottom and did not contact its top part to be sliced.

Figure 6b−f displays low-resolution MS images of five metabolites (m/z = 228.1813, m/z = 337.1691, m/z = 365.1024, m/z = 404.1733 and m/z = 480.2012), which were obtained by traditional LA-ESI-MSI. Each pixel represents the MS signal of a single laser ablation. The

https://doi.org/10.1021/acs.analchem.2c01942
Anal. Chem. XXXX, XXX, XXX−XXX

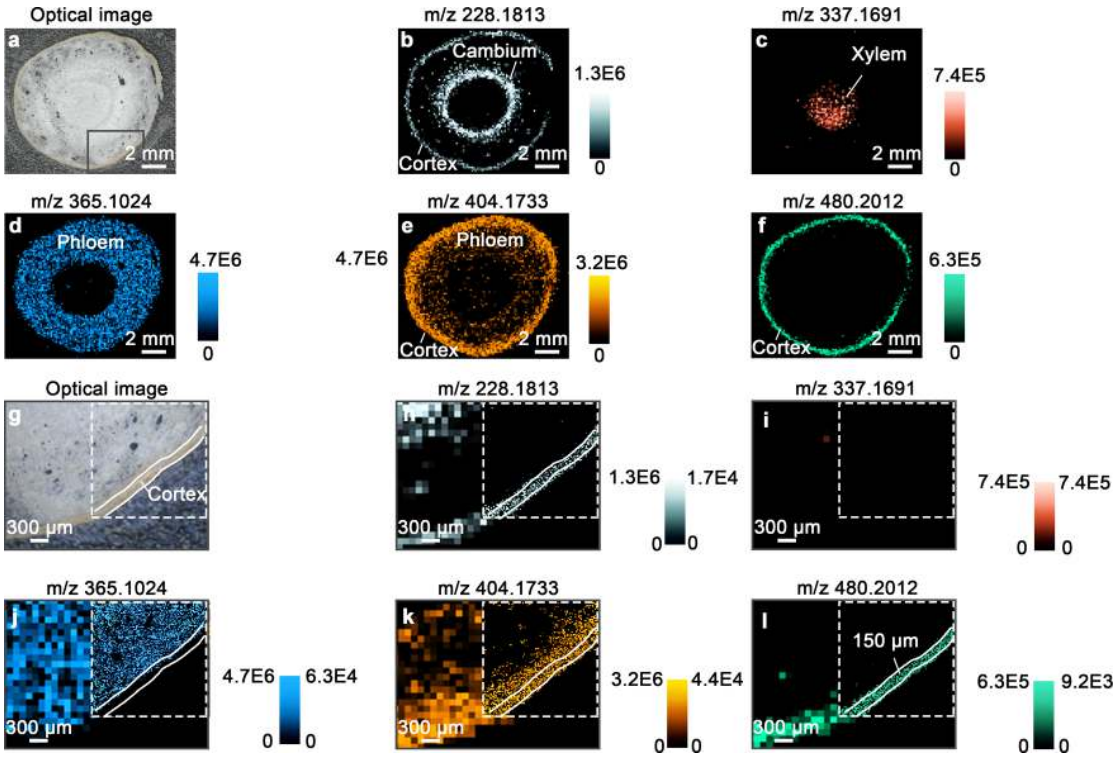

Figure 6. MSI of a parsnip root tissue slice. (a) Optical image of the tissue slice. (b–f) Low-resolution MSI images of selected peaks at m/z = 228.1813, m/z = 337.1691, m/z = 365.1024, m/z = 404.1733, and m/z = 480.2012. (g) Zoom-in optical image of the outlined region in (a). (h–l) Comparison LA-ESI-MSI results for low resolution (left) and high resolution (right). In each color bar shown, the values on the left refer to low resolution and on the right to high resolution.

distribution and relative concentration of each metabolite can be clearly distinguished. The scanned area was 14 mm × 12 mm, and the sample moving step size was set as 100 μm, that is, there are 140 × 120 pixels in each MS image. According to the optical image, the cross section of the parsnip can be divided into four parts from inside to outside, xylem, cambium, phloem, and cortex.[31−33] Although the distribution of different metabolites can be identified, the low-resolution images are generally blurry. Figure 6g shows the magnified image of the region outlined in Figure 6a. We performed the high-resolution MSI with the microlensed fiber in the area inside the dotted line (2 mm × 2 mm) and compared the results of different spatial resolutions. Each pixel represents the MS signal of a microlensed fiber sampling crater with a diameter of ~5 μm. From the high-resolution MS image, the precise location of different molecules can be obtained. For example, the metabolite with m/z = 228.1813 was mainly distributed in the cambium and some traces were also found in the cortex (Figure 6b,h); the ion selected with m/z = 337.1691 was only found in the xylem (Figure 6c,i). Due to the fuzzy boundary, it is difficult to recognize whether the metabolite with m/z = 365.1024 is distributed only in the phloem or both phloem and cortex according to the low-resolution MS image. By comparing the high-resolution MS image with the optical image, we can clearly see that it is only distributed in the phloem (Figure 6j). The ion selected with m/z = 404.1733 is distributed mainly in the cortex but penetrates slightly into the inner phloem (Figure 6k). The metabolite with m/z = 480.2012 is only located in the cortex, which has a thickness of about 150 μm (Figure 6l). Due to the effect of sampling amount, the signal intensity of the high-resolution image is nearly 2 orders of magnitude lower than that of the low-resolution image.

CONCLUSIONS

In mass spectrometric imaging (MSI), high spatial resolution is a long-sought goal. The technique of microlensed fiber LA-ESI-MSI that we have developed in this research is like a chemical microscope, which can illuminate diversities and precise details on the surface of a sample and provide an opportunity for microzone analysis. Our experiment has demonstrated that the spatial resolution of traditional LA-ESI-MSI can be improved by a factor of 20 using the microlensed fiber. Due to the universality, low cost, and operability, it is easy for this technique to be employed for imaging in multiple applications, such as those that occur in clinical medicine and plant biology. It has the potential to reveal specific molecules and metabolites at subcellular resolution. It is worth mentioning that, 5 μm spatial resolution is not the limiting level. The resolution can be further improved if the transport and ionization efficiency of ions can be improved.

ASSOCIATED CONTENT

Supporting Information

The Supporting Information is available free of charge at https://pubs.acs.org/doi/10.1021/acs.analchem.2c01942.

Microscope photographs of the ion source and key parameters of the assembled ion source, real-time observation of the sample and microlensed fiber, and other high-resolution MSI samples (PDF)

https://doi.org/10.1021/acs.analchem.2c01942
Anal. Chem. XXXX, XXX, XXX−XXX

AUTHOR INFORMATION

Corresponding Author

Richard N. Zare − *Department of Chemistry, Stanford University, Stanford, California 94305, United States;* orcid.org/0000-0001-5266-4253; Email: zare@stanford.edu

Authors

Yifan Meng − *Department of Chemistry, Stanford University, Stanford, California 94305, United States*

Xiaowei Song − *Department of Chemistry, Stanford University, Stanford, California 94305, United States*

Complete contact information is available at: https://pubs.acs.org/10.1021/acs.analchem.2c01942

Author Contributions

†Y.M. and X.S. contributed equally to this work. All authors participated in the writing of this manuscript.

Notes

The authors declare no competing financial interest.

ACKNOWLEDGMENTS

The authors thank the Air Force Office of Scientific Research for support through the Multidisciplinary University Research Initiative (MURI) program (AFOSR FA9550-21-1-0170), the National Science Foundation (FAIN: 2028776), and the Stanford Center for Asian Health Research and Education (CARE) for a 2021 seed grant.

REFERENCES

(1) McDonnell, L. A.; Heeren, R. M. A. *Mass Spectrom. Rev.* **2007**, *26*, 606−643.
(2) Niehaus, M.; Soltwisch, J.; Belov, M. E.; Dreisewerd, K. *Nat. Methods* **2019**, *16*, 925−931.
(3) Lu, Q.; Hu, Y.; Chen, J.; Jin, S. *Anal. Chem.* **2017**, *89*, 8238−8243.
(4) Zhao, C.; Xie, P.; Yong, T.; Wang, H.; Chung, A. C. K.; Cai, Z. *Anal. Chem.* **2018**, *90*, 3196−3204.
(5) Meng, Y.; Cheng, X.; Wang, T.; Hang, W.; Li, X.; Nie, W.; Liu, R.; Lin, Z.; Hang, L.; Yin, Z.; Zhang, B.; Yan, X. *Angew. Chem., Int. Ed.* **2020**, *59*, 17864−17871.
(6) Chen, S.; Xiong, C.; Liu, H.; Wan, Q.; Hou, J.; He, Q.; Badu-Tawiah, A.; Nie, Z. *Nat. Nanotechnol.* **2015**, *10*, 176−182.
(7) Xue, J.; Liu, H.; Chen, S.; Xiong, C.; Zhan, L.; Sun, J.; Nie, Z. *Sci. Adv.* **2018**, *4*, No. eaat9039.
(8) Fenn, J. B.; Mann, M.; Meng, C. K.; Wong, S. F.; Whitehouse, C. M. *Science* **1989**, *246*, 64−71.
(9) Fenn, J. B.; Mann, M.; Meng, C. K.; Wong, S. F.; Whitehouse, C. M. *Mass Spectrom. Rev.* **1990**, *9*, 37−70.
(10) Takáts, Z.; Wiseman, J. M.; Gologan, B.; Cooks, R. G. *Science* **2004**, *306*, 471−473.
(11) Ifa, D. R.; Wu, C.; Ouyang, Z.; Cooks, R. G. *Analyst* **2010**, *135*, 669−681.
(12) Venter, A.; Sojka, P. E.; Cooks, R. G. *Anal. Chem.* **2006**, *78*, 8549−8555.
(13) Campbell, D. I.; Ferreira, C. R.; Eberlin, L. S.; Cooks, R. G. *Anal. Bioanal. Chem.* **2012**, *404*, 389−398.
(14) Nemes, P.; Vertes, A. *Anal. Chem.* **2007**, *79*, 8098−8106.
(15) Nemes, P.; Barton, A. A.; Li, Y.; Vertes, A. *Anal. Chem.* **2008**, *80*, 4575−4582.
(16) Stolee, J. A.; Shrestha, B.; Mengistu, G.; Vertes, A. *Angew. Chem., Int. Ed.* **2012**, *51*, 10386−10389.
(17) Nemes, P.; Barton, A. A.; Vertes, A. *Anal. Chem.* **2009**, *81*, 6668−6675.
(18) Yin, Z.; Cheng, X.; Liu, R.; Li, X.; Hang, L.; Hang, W.; Xu, J.; Yan, X.; Li, J.; Tian, Z. *Angew. Chem., Int. Ed.* **2019**, *58*, 4541−4546.
(19) Wang, J.; Wang, Z.; Liu, F.; Cai, L.; Pan, J.-b.; Li, Z.; Zhang, S.; Chen, H.-Y.; Zhang, X.; Mo, Y. *Anal. Chem.* **2018**, *90*, 10009−10015.
(20) Kuznetsov, I.; Filevich, J.; Dong, F.; Woolston, M.; Chao, W.; Anderson, E. H.; Bernstein, E. R.; Crick, D. C.; Rocca, J. J.; Menoni, C. S. *Nat. Commun.* **2015**, *6*, No. 6944.
(21) Zavalin, A.; Todd, E. M.; Rawhouser, P. D.; Yang, J.; Norris, J. L.; Caprioli, R. M. *J. Mass Spectrom.* **2012**, *47*, 1473−1481.
(22) West, R. E.; Findsen, E. W.; Isailovic, D. *J. Am. Soc. Mass Spectrom.* **2013**, *24*, 1467−1476.
(23) Meng, Y.; Gao, C.; Lu, Q.; Ma, S.; Hang, W. *ACS Nano* **2021**, *15*, 13220−13229.
(24) Meng, Y.; Ma, S.; Zhang, Z.; Hang, W. *Anal. Chem.* **2020**, *92*, 9916−9921.
(25) Shrestha, B.; Vertes, A. *Anal. Chem.* **2009**, *81*, 8265−8271.
(26) Shrestha, B.; Patt, J. M.; Vertes, A. *Anal. Chem.* **2011**, *83*, 2947−2955.
(27) Boughton, B. A.; Thinagaran, D.; Sarabia, D.; Bacic, A.; Roessner, U. *Phytochem. Rev.* **2016**, *15*, 445−488.
(28) Bartels, B.; Svatoš, A. *Front. Plant Sci.* **2015**, *6*, No. 471.
(29) Kulkarni, P.; Wilschut, R. A.; Verhoeven, K. J. F.; van der Putten, W. H.; Garbeva, P. *Planta* **2018**, *248*, 1515−1523.
(30) Stopka, S. A.; Wood, E. A.; Khattar, R.; Agtuca, B. J.; Abdelmoula, W. M.; Agar, N. Y. R.; Stacey, G.; Vertes, A. *Anal. Chem.* **2021**, *93*, 9677−9687.
(31) Hacke, U. G.; Sperry, J. S. *Perspect. Plant Ecol. Evol. Syst.* **2001**, *4*, 97−115.
(32) Lachaud, S.; Catesson, A.-M.; Bonnemain, J.-L. *C. R. Acad. Sci., Ser. 3* **1999**, *322*, 633−650.
(33) Lu, Q.; Xu, Z.; You, X.; Ma, S.; Zenobi, R. *Anal. Chem.* **2021**, *93*, 6232−6238.